

A compact radiofrequency drive based on interdependent resonant circuits for precise control of ion traps

Cite as: Rev. Sci. Instrum. **90**, 023201 (2019); <https://doi.org/10.1063/1.5063305>

Submitted: 26 September 2018 . Accepted: 22 January 2019 . Published Online: 11 February 2019

Amelia Detti, Marco De Pas,  Lucia Duca,  Elia Perego, and  Carlo Sias



View Online



Export Citation



CrossMark

ARTICLES YOU MAY BE INTERESTED IN

[A scalable hardware and software control apparatus for experiments with hybrid quantum systems](#)



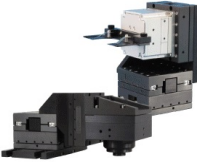
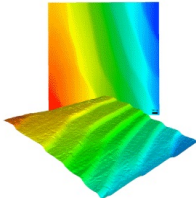
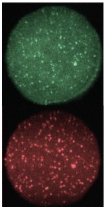
Review of Scientific Instruments **89**, 113116 (2018); <https://doi.org/10.1063/1.5049120>

[Low power RF amplifier circuit for ion trap applications](#)

Review of Scientific Instruments **87**, 094704 (2016); <https://doi.org/10.1063/1.4962707>

[A cryogenic radio-frequency ion trap for quantum logic spectroscopy of highly charged ions](#)

Review of Scientific Instruments **90**, 073201 (2019); <https://doi.org/10.1063/1.5100594>

 MCL MAD CITY LABS INC. www.madcitylabs.com	<p>Nanopositioning Systems</p> 	<p>Modular Motion Control</p> 	<p>AFM and NSOM Instruments</p> 	<p>Single Molecule Microscopes</p> 
---	--	--	---	--

A compact radiofrequency drive based on interdependent resonant circuits for precise control of ion traps

Cite as: Rev. Sci. Instrum. 90, 023201 (2019); doi: 10.1063/1.5063305
Submitted: 26 September 2018 • Accepted: 22 January 2019 •
Published Online: 11 February 2019



Amelia Detti,^{1,2,a)} Marco De Pas,^{1,3} Lucia Duca,²  Elia Perego,^{2,4}  and Carlo Sias^{2,3,5} 

AFFILIATIONS

¹Università degli Studi di Firenze, Dipartimento di Fisica e Astronomia, Via G. Sansone 1, I-50019 Sesto Fiorentino, Italy

²Istituto Nazionale di Ricerca Metrologica, Strada delle Cacce 91, I-10135 Torino, Italy

³European Laboratory for Nonlinear Spectroscopy, Via N. Carrara 1, I-50019 Sesto Fiorentino, Italy

⁴Politecnico di Torino, Corso Duca degli Abruzzi 24, I-10129 Torino, Italy

⁵INO-CNR, Via N. Carrara 1, I-50019 Sesto Fiorentino, Italy

^{a)}Electronic mail: detti@lens.unifi.it

ABSTRACT

Paul traps are widely used to confine electrically charged particles like atomic and molecular ions by using an intense radiofrequency (RF) field, typically obtained by a voltage drop on capacitive electrodes placed in vacuum. We present a RF drive realized on a compact printed circuit board and providing a high-voltage RF signal to a quadrupole Paul trap. The circuit is formed by using four interdependent resonant circuits – each of which is connected to an electrode of a Paul trap – fed by low-noise amplifiers, leading to an output voltage of peak-to-peak amplitude up to 200 V at 3.23 MHz. The presence of a single resonant circuit for each electrode ensures a strong control on the voltage drop on each electrode, e.g., by applying a DC field through a bias tee. Additionally, the moderate quality factor $Q = 67$ of the resonant circuits ensures a fast operation of the drive, which can be turned on and off in less than $10 \mu\text{s}$. Finally, the RF lines are equipped with pickups that sample the RF in phase and amplitude, thus providing a signal that can be used to actively control the voltage drop at the trap's electrodes.

© 2019 Author(s). All article content, except where otherwise noted, is licensed under a Creative Commons Attribution (CC BY) license (<http://creativecommons.org/licenses/by/4.0/>). <https://doi.org/10.1063/1.5063305>

I. INTRODUCTION

Paul traps are one of the most exceptional tools in the field of experimental quantum physics.¹ By applying a radiofrequency (RF) signal to one or more electrodes, it is possible to create a deep attractive potential capable of trapping ideally anything possessing an electric charge, from macroscopic objects² to atomic and molecular ions.³ Charged particles can be trapped for a considerably long time, especially with the use of laser cooling techniques, making arrays of cold ions confined in a Paul trap one of the most promising hardware for the realization of quantum technologies.⁴ In its linear configuration, a Paul trap is formed by two pairs of parallel, linear electrodes (e.g., rods) that are equally spaced. Opposite

electrodes are placed at the same voltage in order to create an electric quadrupole field at the center of the trap. Trapping is achieved when one pair of electrodes is connected to ground, while the second one is placed at a voltage $V_0 \sin(\Omega_T t)$. In an alternative configuration, a pair of opposite electrodes is fed with a voltage $V_0/2 \sin(\Omega_T t)$, while the second pair is placed at $V_0/2 \sin(\Omega_T t + \pi)$. Both configurations lead to an attractive harmonic pseudo-potential of frequency,⁵

$$\omega_r = \frac{q}{\sqrt{2}m} \frac{V_0}{r_0^2 \Omega_T}, \quad (1)$$

where q is the particle's charge, m is its mass, r_0 is the distance between the center of the trap and the electrodes, and

$\omega_r \ll \Omega_T$. For most applications in ion trapping, a trapping frequency $\omega_r > 1$ MHz is highly desirable. It facilitates the optical control of the ion motional state in the trap,⁶ it permits to reach more easily the Lamb-Dicke regime, and it reduces the effects of the so-called “anomalous heating”.⁷ To this end, a relatively large amplitude of the RF potential is needed. In a non-miniaturized trap, for instance, a typical distance between the electrodes ranges from 100s μm to a few mm, and the amplitude of the RF needed must range from a few hundreds to thousands of volts. For a given amplitude of RF, the frequency of the secular motion can be maximized by using a differential drive in which all the electrodes are fed with an RF signal having the right phase.

One of the main challenges in realizing a Paul trap is finding a way to feed the electrodes with such a large oscillating voltage. A common strategy is to realize a resonant circuit in which the ion trap – playing the role of the capacitance – is connected in series to an inductor.⁸ This approach has two advantages: on the one hand, there is no need of high power since the amplification is provided by the resonance of the resulting LC circuit; on the other hand, the resonant circuit plays the role of a filter, thus reducing the effects of the noise associated with the primary source. In order to maximize both effects, the quality factor Q of the resonator should be as large as possible. To this end, the resonant circuit must have a large inductance and a low resistance, while the capacitance should be ideally provided only by the ion trap, in order to maximize the voltage drop across the electrodes.

In a typical implementation, the inductance is provided by a helical resonator, formed by a few windings of copper wire surrounded by a conducting shield.^{9,10} However, this device usually has a relatively large size, which poses difficulties in the design of a compact experimental setup. As a result, increasing interest has been devoted to the miniaturization of RF drives into printed circuit boards (PCBs),¹¹ for instance, by using logic CMOS inverters¹² or low noise amplifiers.¹³

In this paper, we present an RF drive realized on a PCB and formed by a network of four resonant circuits – each connected to a single electrode of a linear Paul trap – in which the high voltage output is obtained with the combination of a resonant RLC circuit and a low-noise commercial amplifier. The four resonant circuits are interconnected in order to ensure the existence of a common resonant mode with the same frequency and amplitude. This design, which differs from other RF drives recently realized on PCBs,¹¹⁻¹³ ensures that an independent DC field can be provided to each of the four RF outputs with a bias tee. This condition is particularly important in applications in which an excellent compensation of micromotion is needed,^{14,15} e.g., in atom-ion physics experiments.¹⁶ Finally, the RF drive is provided with two different kinds of pickup probes, which continuously measure both the amplitude and the phase of the RF. These signals can be used to monitor the voltage generated by the drive and to actively stabilize the potential acting on the ions.¹⁷ Each resonant circuit has a quality factor $Q \sim 67$, but the combination with a low

power amplifier ensures an overall increase in the voltage by a factor ~ 200 . The moderately small Q of each resonant circuit ensures a fast operation of the drive, a property that can be relevant in experiments in which the trapping potential has to be quickly turned off, e.g., for transferring a particle from a Paul trap to an optical trap.¹⁸

The paper is organized as follows: in Sec. II, we present the conceptual design of the interdependent resonant circuits. In Sec. III, we show the RF board, while in Sec. IV we present some measurements of characterization of the board. Finally, Sec. V is devoted to the conclusions.

II. RESONANT CIRCUIT DESIGN

The RF drive is formed by four resonant circuits – one per electrode of a Paul trap – that amplify and filter the RF signal. The resonant circuits are interconnected in the RF drive in order to enforce a common resonating frequency. In this section, we provide a detailed description of the characteristics of each resonant circuit and of how they are combined in the RF board.

A. The single resonating circuit

The fundamental circuit of the RF drive is an RLC circuit resonating at the frequency $\Omega_T = \sqrt{1/L_{\text{eq}}C_{\text{eq}}}$, where L_{eq} and C_{eq} are the equivalent inductance and capacitance of the whole circuit, respectively. The quality factor of this circuit is

$$Q = \frac{1}{R} \sqrt{\frac{L_{\text{eq}}}{C_{\text{eq}}}}, \quad (2)$$

with R being the equivalent series resistance. If we imagine to feed this circuit with a signal of frequency Ω_T and amplitude $V_0/2$, for instance through a transformer, the voltage drop at the capacitor of the RLC circuit is $V_0/2 \sin(\Omega_T t)$. The circuit is designed such that the capacitive load C_{eq} is mainly due to the capacitance of the RF electrode. Its value is considered to be a fixed quantity since it depends on the Paul trap geometry, i.e., the electrode's shape, size, and the distance from the other electrically conductive parts. The equivalent inductance L_{eq} , instead, is a free parameter that can be tuned in order to find the best compromise between a large quality factor Q and a relatively large resonant frequency Ω_T . Additionally, and independently from the resonant frequency, the quality factor is increased by reducing the total resistance R , which should be ideally kept as low as possible.

A possible strategy for realizing a sufficiently large inductance – e.g., on the order of a few 100s μH – without implementing a bulky helical resonator is to build inductors by winding a conducting wire on a ferrite core. Ferrite cores are characterized by a frequency-dependent magnetic permeability that depends on the material, the size, and the shape of the core. While the reactive term of the impedance is proportional to the real part of the magnetic permeability, its imaginary part provides a resistive term, physically caused by the eddy currents induced in the core. In general, the resistive and reactive parts are linked by the dissipation factor DF ,

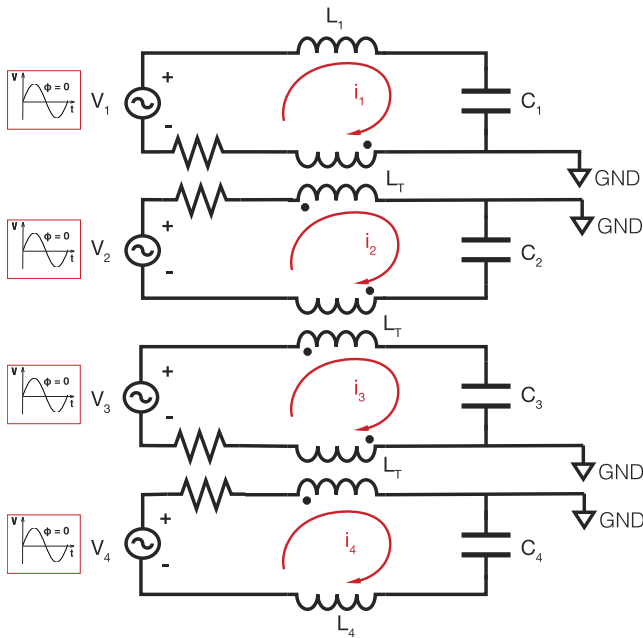


FIG. 1. Schematic of the RF drive representing the conceptual idea behind the design. Four resonant RLC circuits feed four capacitors — representing the total capacitance of the ion trap plus the drive circuit — at an iso-frequency Ω_T . The voltage provided by the sources is depicted in the insets on the left.

a specific characteristic of the core material. The presence of the inductors' resistive term affects the overall resistance R of the RLC circuit, which then reads

$$R = R_0 + \Omega_T L_{eq} DF, \quad (3)$$

where R_0 is the component of R that does not depend on the drive frequency, originating, for example, from the wires' resistance. Other possible frequency-dependent terms of the resistance, for instance, due to the skin effect on the wires, have for the moment been neglected. The quality factor of the RLC circuit can then be re-written in the form

$$Q = \frac{1}{R_0 \Omega_T C_{eq} + DF}. \quad (4)$$

In the low resistance regime ($R_0 \Omega_T C_{eq} \ll DF$), the real limitation to the Q factor is the dissipation factor DF : in order to keep a high value of Q , it is crucial to choose a ferrite with the lowest possible losses.

The passive RLC circuit must be fed with RF produced by using a primary source, typically a synthesizer. The connection between the primary source and the RLC resonator, or “secondary circuit,” can be realized by using a transformer. Intuitively, one may imagine that – in order to transfer as much power as possible – the secondary circuit must be impedance-matched to the primary one (which has typically an impedance $Z_S = 50 \Omega$). This implies that at resonance, i.e., when the reactive part of the RLC circuit is zero, the real part of the inductance should be matched to Z_S with an additional circuit connected to the primary source. However, if $\text{Re}[Z_S]$ is smaller than R , impedance matching causes a decrease in the quality factor since $\text{Re}[Z_S] + R < 2R$.

As a result, in the case $\text{Re}[Z_S] < R$, it is more convenient not to match the impedances of the primary and secondary circuits since there is not any particular constraint on the current circulating in the drive, but there is the need to have a high Q and a low dissipation on the electrodes. The drawbacks for the mismatch are a higher dissipated power on the source – a synthesizer with a high-power low-impedance

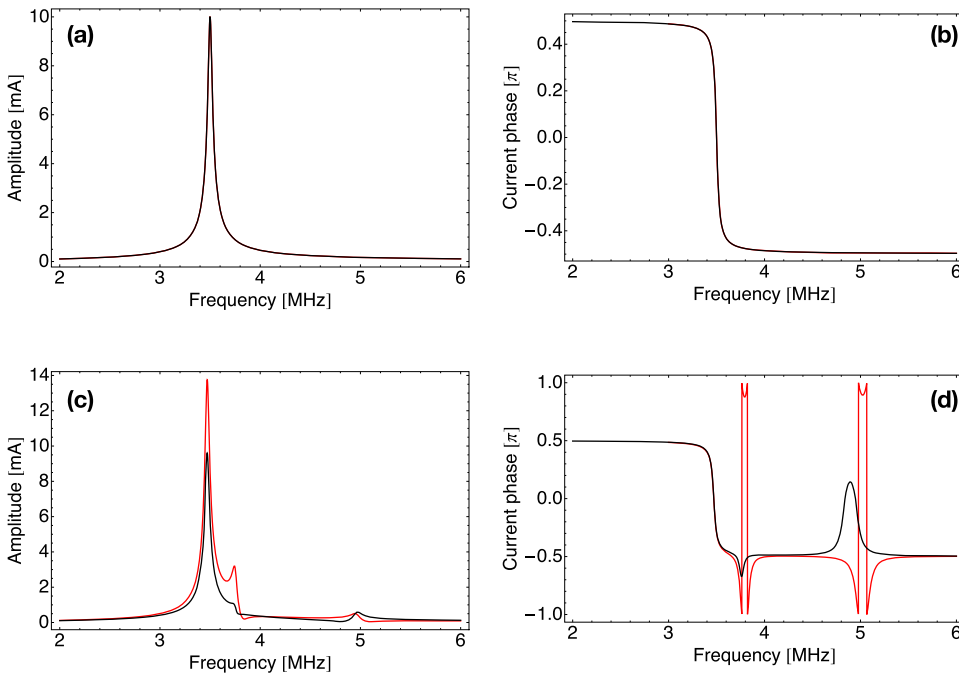


FIG. 2. Simulated amplitude and phase of the current circulating in the circuit as a function of the frequency. Plots (a) and (b) show the current's amplitude and phase in the four resonant circuits in which all the capacitances are equal to $C_{eq} = 5.6 \text{ pF}$, all the resistances are set to 100Ω , and $L_1 = L_2 = L_{eq}/2$, $L_T = L_{eq}/4$, $L_{eq} = 370 \mu\text{H}$, with L_T being the transformers' mutual inductances. Plots (c) and (d) show the amplitude and phase of the current i_1 (red line) and i_2 (black line) in a circuit in which the electric components have the same values as in the plots (a) and (b), except for $C_1 = 1.1 C_{eq}$ and $C_2 = 0.9 C_{eq}$.

amplifier – rather than on the trap and the possible presence of reflections creating stationary waves on the resonant lines, resulting in a DC offset on the RF electrode. However, this effect can be counter-acted by adding to the RF signal an external DC field.

B. The interdependent four resonant circuits

Each electrode of a Paul trap can be modelled as a capacitive load. However, it is reasonable to associate with it also an equivalent series resistance (ESR), which may originate, e.g., from the dielectric losses of the electrode's insulating support. Ideally, capacitance and resistance should be the same for each electrode; in practice, this is never exactly true due to possible asymmetries in the trap assembly or to mechanical imperfections. This makes it practically very hard to realize four independent RLC circuits having the same resonant frequency. Our strategy to ensure the presence of a common resonant frequency is to place 1:1 transformers that connect the four resonant circuits (see Fig. 1). We use commercial software (Mathematica and LTSpice) to simulate this configuration, in which we consider only the resonant RLC circuits connected to an ideal RF source. The results of the Mathematica simulation are shown in Fig. 2. If one assumes that the electrodes are exactly equal, there is only one common resonance frequency Ω_T , as expected. Furthermore, the RF signal in neighbour circuits has opposite phase, so the board generates in overall two pairs of identical RF signals with opposite phase, as requested for a correct functioning of the Paul trap. In case a small difference between the capacitances of the electrodes is introduced, a number of minor resonances appear, but the common resonant frequency holds, proving that this circuit design is robust against small variations of the electrical components.

These data were furthermore compared with simulations on LTSpice which gave, up to a few percent deviations, the same quantitative result.

III. THE RF DRIVE PROTOTYPE

We have realized an RF drive based on the scheme presented in Sec. II B. The scheme is divided in five main “blocks” (see Fig. 3). Block **A** represents the part of the circuit that is placed inside an ultra-high vacuum chamber, i.e., the capacitances and the ESRs of the Paul trap electrodes. The actual values of the capacitances and the ESRs there reported are relative to the Paul trap for which this RF drive was initially designed, and they were estimated by simulating the trap with a finite element software (Comsol Multiphysics). Block **B** represents the portion of the secondary circuits that is placed outside the vacuum chamber: blocks **A** and **B** constitute four interdependent RLC circuits. The inductances in block **B** are designed to resonate at approximately $\Omega_T = 2\pi \times 3.5$ MHz. This frequency was chosen in order to maximize the quality factor for a given value of C_{eq} , DF , and R_0 [see Eq. (4)] while keeping the RF frequency reasonably large in order to ensure a successful trapping of the ion. Block **C** is formed by four 1:4 transformers that are used to connect the primary and the secondary circuits, i.e., to feed the resonant lines with a RF signal. The purpose of these step-up transformers is to increase by a factor $a = 4$ the voltage amplitude from the primary to the secondary circuit, thereby enhancing the total amplification factor.

Conceptually, the RF sources of Fig. 1 are realized by blocks **D** and **E**. Block **E** is constituted by four independent Direct Digital Synthesis (DDS) chips that are set at a frequency $\Omega_T/2\pi$ and have tunable amplitudes and phases.

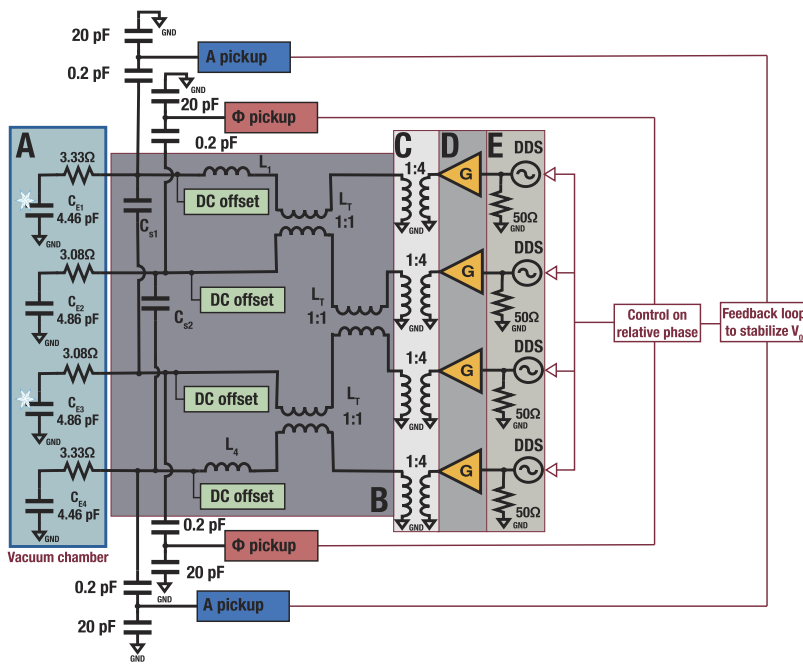


FIG. 3. Simplified block diagram of the complete RF drive. **A** Electrodes of a Paul trap, considered as a series of a capacitance and a resistance. The values in figure are obtained by simulating with COMSOL Multiphysics the Paul trap for which this RF drive was designed. Electrodes marked with a star are out of phase with respect to the other two. **B** Iso-frequency resonant lines with pickups for phase and amplitude stabilization, balancing capacitors C_{S1} and C_{S2} and DC offset inputs. **C** 1:4 step-up transformers that inductively couple the resonant circuits to the RF sources. **D** Low-impedance op-amps for pre-amplification of the input signals. **E** Four independent DDS sources providing the RF signals with tunable amplitude and phase. The complete schematic can be found in Ref. 19.

In our realization, block **E** is not placed on the RF drive board, but it is embedded in the control system of the experiment.²⁰ The DDSs are connected to four amplifiers (block **D** – Analog Devices AD8392) characterized by an output impedance of $R_S = 0.2 \Omega$ at $\Omega_T = 2\pi \times 3.5$ MHz. The amplifiers' input impedance is matched to the 50Ω output of the DDSs.

The op-amps are set for a feedback gain of $G \approx 5$. This choice ensures an increase in the signal enhancement at resonance since the real part of the impedance of the circuit is reduced. If we consider the pre-amplification stage and the step-up transformers, the Q factor of Eq. (4) becomes

$$Q = \frac{1}{(R_0 + a^2 R_S) \Omega_T C_{eq} + DF} \quad (5)$$

The magnetic cores used for the inductors of the RF drive are toroidal Ni-Zn ferrite cores (material: DN5H from the company DMEGC), which are characterized by a low dissipation factor around Ω_T . In order to estimate the cores' dissipation factor, we have realized a number of resonant circuits formed by a single inductor and a conventional capacitor resonating at approximately Ω_T . With these circuits, we have measured the resistance at resonance as a function of the impedance of the inductor. The results are plotted in Fig. 4. A dissipation factor $DF = (8.0 \pm 0.2) \times 10^{-3}$ is obtained from a linear fit to the data. By substituting this value in Eq. (5), we can estimate $Q \approx 115$ and a resonance frequency of $\Omega_T = 2\pi \times 3.5$ MHz. We notice that the dissipation factor DF is the largest term in the denominator of Eq. (5), and therefore the dissipation of the core represents the strongest limitation to the Q factor of this RF drive.

Since the capacitance and the ESR of the electrodes are in general not identical, we have placed two balancing capacitors C_{S1} and C_{S2} that connect the in-phase lines of the drive

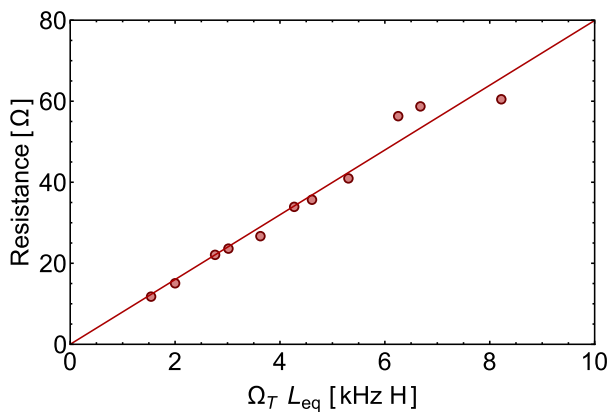


FIG. 4. Calibration of the dissipation factor DF for DN5H toroidal ferrite cores of height 6 mm, internal radius 10 mm, and external radius 18 mm. The copper wire used had a diameter of 0.2 mm. Each point in the plot corresponds to the resistance at resonance of an RLC circuit formed by a ceramic capacitor and a homemade inductor. The values of resistance, inductance, and resonant frequency are obtained with a vector network analyzer. The dependence of the total resistance as a function of L_{eq} and Ω_T is extracted. The value $DF = 0.0080 \pm 0.0002$ is extracted from the linear fit to the data.

in order to ensure that the RF signals of the secondary circuits all have the same amplitude. Moreover, we have equipped the RF drive with phase and amplitude pickups that can be used to perform active stabilization of the RF signal, with the goal of counter-acting possible effects – like thermal fluctuations of the different elements of the drive – that may affect the long-term stability of the trap frequency ω_r .¹⁷ The active stabilization of the RF potential requires a faithful sampling of the voltage drop at the electrodes. This needs to be performed in a section of the circuit that is at a high impedance load. To this end, we implemented little-invasive probes with 1:100 capacitive dividers realized with the 0.2 pF and 20 pF capacitors as the last elements of the circuit outside the vacuum (see Fig. 3 and the complete drive schematic in Ref. 19). We chose the value of the capacitors in order to extract approximately 1% of the signal without affecting the resonance since the impedance of the capacitive dividers is much larger than the lines' impedance. The capacitive dividers are realized by placing commercial surface mount device (SMD) capacitors as close as possible to the lines in order to suppress the capacitive effects of the additional lines. We separately tested inductive probes based on parallel lines placed at a side or below the RF output lines in the PCB, but we observed a strong cross talk between each pickup and all four RF lines. The capacitive dividers work as phase pickups (ϕ -pickups) that carry information on the resonance frequency Ω_T and the relative phase between the signals on the RF electrodes. The amplitude pickups (A-pickups) are realized by placing a rectifier, not shown in Fig. 3, after the capacitive divider to generate a signal linearly dependent on the RF amplitude $V_0/2$.¹⁷ The pickup electronics can be found in the full drive schematic.¹⁹ The board has one A-pickup and one ϕ -pickup for both pairs of electrodes at $V_0/2 \sin(\Omega_T t)$ and at $V_0/2 \sin(\Omega_T t + \pi)$. The pickup signals can be used to actively stabilize both the trap frequency and the relative phase between the electrodes.

IV. CHARACTERIZATION OF THE RF DRIVE

We have realized the RF drive on a 4-layer PCB of size approximately 100 mm \times 70 mm (see Fig. 5). The operation of the board was first characterized by substituting the electrodes with 5.6 pF ceramic capacitors. This choice allowed us to directly monitor the RF signal with external probes, if needed.

Figure 6 shows the amplitude of the RF signal in the secondary circuit as a function of the frequency of the primary RF source. The circuit has several resonances, including the one at $\Omega_T = 2\pi \times 3.37$ MHz that we had initially targeted as the working resonance and that we expected from the simulation to be at approximately $2\pi \times 3.5$ MHz. The resonance at Ω_T has a full width at half maximum of $2\pi \times 91$ kHz, which we extracted from a Lorentzian fit. The resulting quality factor is $Q = 57$, which is lower than what is expected from Eq. (5). We attribute this discrepancy to the non-ideal behavior of the transformers that have a mutual inductance coefficient smaller than 1. Other effects that may reduce the quality factor of the circuit are possible cross talks between

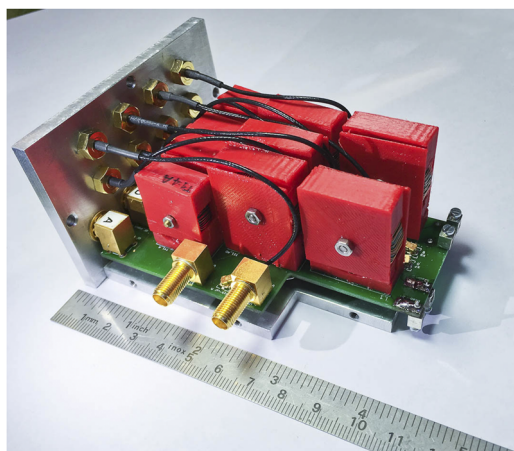


FIG. 5. Picture of the RF drive implemented on a 4-layer PCB. The blocks **B**, **C**, and **D** of Fig. 3 are implemented on the board. The home-made inductors are encapsulated in small plastic cases (in red) in order to avoid capacitive couplings with the PCB conducting planes.

transformers that are closely placed on the board. We notice that the value of the quality factor could be increased, e.g., by changing the inductors of the board, at the price of lowering the resonant frequency Ω_T . The relatively small quality factor ensures a fast operation of the drive: we measure a falling time at resonance of $7.7 \mu\text{s}$, corresponding to a time constant $\tau = 3.5 \mu\text{s}$.

In addition to the resonance at Ω_T , other resonances arise at different frequencies (see Fig. 6). We attribute the presence of these resonances to the small unbalancing between the four resonant circuits, the components of which are not perfectly

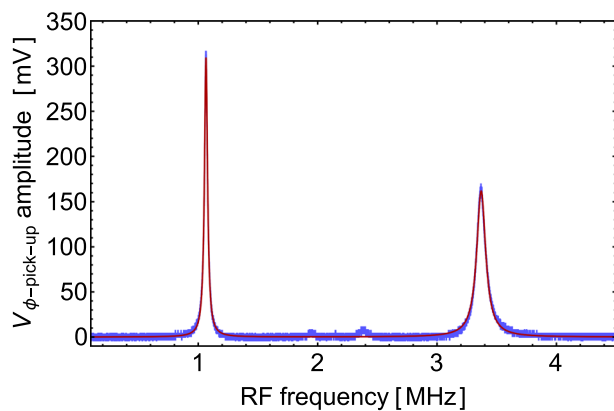


FIG. 6. Plot of the drive response tested with 5.6 pF ceramic capacitors emulating the trap electrodes. The frequency of the input RF signals is swept to observe the main resonances of the circuit. The peak-to-peak amplitude of the RF signal reaching C_{E2} is detected via the ϕ -pickup output and fitted with a Lorentzian curve (red) to extract the linewidth. Among all the resonances, the one at 3.37 MHz is the only one for which the RF signals of the four secondary circuits have the right phase relation.

equal. This speculation was confirmed by simulating the circuit with the commercial software LTSpice, in which a small variation of one of the components of the circuit results in the appearance of new resonances. Of all the additional resonances, we further investigated the strongest one at about 1.06 MHz . This resonance corresponds to the creation of four RF signals all having the same phase. This condition clarifies the appearance of this resonance at a frequency considerably smaller than Ω_T : since the equivalent inductances associated with the 1:1 transformers in block **B** of Fig. 3 depend on the direction of the currents, a resonance with all the RF signals in phase is characterized by values of L_{eq} that differ with respect to the ones associated with the resonance at Ω_T , resulting in a strong difference in both the frequency and the quality factor of the resonance.

We tested the response of the pickups at resonance. Figure 7 shows the response of the two A-pickups as a function of the amplitude of the primary RF source. The data show a very good linear response. Additionally, we measured the bandwidth of the A-pickups, finding it equal to 6 Hz . This corresponds to the maximum bandwidth for a stabilization loop that can correct slow amplitude variations. If needed, this bandwidth can be changed by modifying the components of the rectifiers. This can be performed at the cost of increasing the ripple amplitude on the pickup signal – currently approximately 15 mV for $V_0 = 200 \text{ V}$. Additionally, we used the ϕ -pickups to measure the relative phase between the RF signals used to feed neighbour electrodes. For maximizing the frequency of the secular potential, this phase should be π . Figure 8 shows the output signals of the two ϕ -pickups when the phase, frequency, and amplitude of the DDSs are set correctly. The sinusoidal signals of frequency Ω_T have a phase difference $\phi/\pi = 0.99435 \pm 0.00004$, measured from fit. This differs only slightly from the ideal value $\phi/\pi = 1$; however, by treating this difference of the relative phase with the same

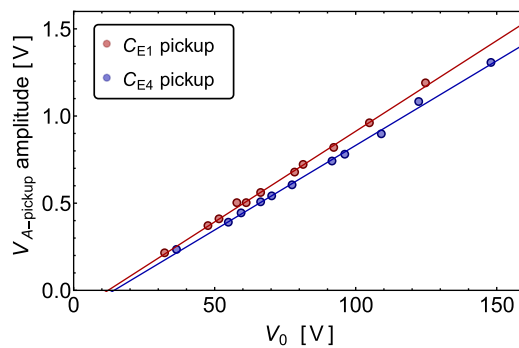


FIG. 7. Linearity test for the two A-pickups sensing the signals reaching C_{E1} and C_{E4} . The measurement is performed by changing the amplitude of the RF signal, $V_0/2$. Experimental data are plotted together with their linear fits, which lead to the slopes $(10.4 \pm 0.2) \times 10^{-3}$ and $(9.7 \pm 0.2) \times 10^{-3}$ for the pickups placed close to C_{E1} and C_{E4} , respectively. The difference between the two curves are due to small mismatches in the values of the electric components forming the capacitive dividers and the rectifiers. The linear fitting functions have a non-zero offset caused by the non-linear behavior at low RF amplitudes of the diodes that are part of the rectifiers.

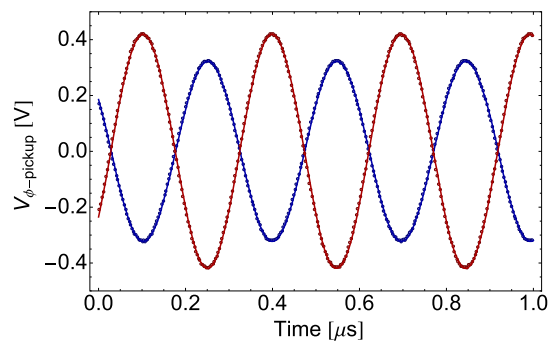


FIG. 8. Phase of the signal outputs. The data show the outputs of the ϕ -pickups probing the signals at the capacitors C_{E2} (red) and C_{E3} (blue). Measurements are taken with the DDS frequencies set to Ω_T . When the phase of the input signals is set correctly, the outputs of the two ϕ -pickups are sinusoidal signals that are out of phase. The sinusoidal fit to the data gives a phase difference $\phi/\pi = 0.994\,35 \pm 0.000\,04$.

approach of Ref. 14, it emerges that this phase mismatch does not provide a contribution to the micromotion, as a phase mismatch affecting signals fed to opposite electrodes would. We note that the amplitude of the two A-pickups and the two ϕ -pickups are different, possibly because of small differences in the components forming the capacitive dividers. These differences can easily be calibrated by using external probes.

At resonance, we are able to produce signals of peak-to-peak amplitude up to $V_0 = 200$ V with an input RF of peak-to-peak amplitude 1 V. We checked the stability of the drive by running it for 24 h at the maximum output without active stabilization. We found no appreciable changes in the resonant frequency, but we noticed a small variation of the phase of the RF signal. These small instabilities, possibly due to thermal effects on the ferrite core, can actively be corrected by probing the signals with the ϕ -pickups. The total power consumption of the board is due to the op-amps and is ~ 2 W. This value, which is calculated for the sum of all four resonant circuits, currently limits the maximum reachable peak-to-peak voltage since a higher power could lead to a failure of the op-amps. We note that the power consumption is nominally higher than other compact drive implementations in the literature. However, the power consumption in these drives is kept low by realizing smaller gains,¹² by running at lower frequencies,¹³ or by working at temperatures for which a cryostat is needed.²¹

Finally, we tested the RF drive when connected to the linear Paul trap that is currently under development at our laboratory. We measure a resonance at $\Omega_T = 2\pi \times 3.23$ MHz, with a full width at half maximum of $2\pi \times 75$ kHz, resulting in a quality factor $Q = 67$. This small variation originates from the fact that in its actual implementation we found the electrodes to have a capacitance of approximately 10 pF, slightly larger than that initially simulated. The resonance frequency does not follow the expected $1/\sqrt{C_{eq}}$ scaling due to the presence of a 37 pF offset capacitance, which we attribute to the

parasitic capacitance between the wire windings around the ferrite cores.

V. CONCLUSIONS

We presented a compact RF drive for ion traps built on a PCB and composed of four interdependent resonant RLC circuits which are capable to work in iso-frequency, iso-amplitude, and proper phase relation. The presence of four resonant circuits, one per electrode of a Paul trap, ensures the possibility of adding to each RF signal a DC voltage through a bias tee. A high voltage output is realized by using a low-noise amplifier and the enhancement factor of the resonant RLC circuits. The drive has a quality factor $Q = 67$ – mainly limited by the dissipation factor of the ferrite material constituting the inductors of the resonant circuits – while the total voltage gain of the whole drive is approximately 200. This gain is sufficiently large to ensure ion trapping while dissipating moderate powers on the op-amps, namely, less than 2 W for four trap electrodes. The drive is also equipped with non-invasive pickups in order to monitor the RF signal amplitude and phase, making it possible to actively stabilize the voltage drop on the electrodes of the Paul trap via feedback loops.

Quantitatively, the performances of the drive in its current realization depend on the specific ion trap to which it is connected. The RF drive can in principle be adapted for higher frequencies and larger RF amplitudes. However, the components of the circuit must be changed accordingly. First, ferrite cores must be chosen in order to have the lowest possible dissipation factor at the resonant frequency. Second, in order to obtain larger RF amplitudes, an alternative amplification stage should be considered since the maximum RF amplitude attainable with the RF drive is currently limited by the power that can be dissipated by the amplifier. For our AD8392 amplifier, the limit is approximately 250 V; in order to reach larger amplitudes, a possible alternative is to use class C transistors, one for each channel. Additionally, the drive scheme can be scaled up to a larger number of inter-connected resonant circuits, e.g., for driving multipole RF traps.²² Finally, the compact PCB size and low power consumption make the drive suitable for transportable ion trap experiments.

ACKNOWLEDGMENTS

We thank Massimo Inguscio for continuous support, the members of the LENS electronic workshop for discussions, and Claudio Calosso for discussions and a critical reading of the manuscript. This work was supported by the ERC-Starting Grant PlusOne (Grant Agreement No. 639242), the SIR grant ULTRACOLDPLUS (Grant No. RBSI14GNS2), the FARE grant UltraCrystals (Grant No. R165JHRWR3), and the European Metrology Programme for Innovation and Research (EMPIR) Project No. 17FUN07 (CC4C). This project has received funding from the EMPIR programme co-financed by the Participating States and from the European Union's Horizon 2020 Research and Innovation programme.

REFERENCES

- ¹W. Paul, *Rev. Mod. Phys.* **62**, 531 (1990).
- ²H. Winter and H. Ortjohann, *Am. J. Phys.* **59**, 807 (1991).
- ³D. Leibfried, R. Blatt, C. Monroe, and D. Wineland, *Rev. Mod. Phys.* **75**, 281 (2003).
- ⁴H. Haeffner, C. Roos, and R. Blatt, *Phys. Rep.* **469**, 155 (2008).
- ⁵D. J. Wineland, C. Monroe, W. M. Itano, D. Leibfried, B. E. King, and D. M. Meekhof, *J. Res. Natl. Inst. Stand. Technol.* **103**(3), 259 (1998).
- ⁶C. Monroe, D. Meekhof, B. King, S. Jefferts, W. Itano, D. Wineland, and P. Gould, *Phys. Rev. Lett.* **75**, 4011 (1995).
- ⁷M. Brownnutt, M. Kumph, P. Rabl, and R. Blatt, *Rev. Mod. Phys.* **87**, 1419 (2015).
- ⁸R. Jones and S. Anderson, *Rev. Sci. Instrum.* **71**, 4335 (2000).
- ⁹W. Macalpine and R. Schildknecht, *Proc. IRE* **47**, 2099 (1959).
- ¹⁰J. D. Siverns, L. R. Simkins, S. Weidt, and W. K. Hensinger, *Appl. Phys. B* **107**, 921 (2012).
- ¹¹R. Mathur and P. O'Connor, *Rev. Sci. Instrum.* **77**, 114101 (2006).
- ¹²Y.-Y. Jau, F. Benito, H. Partner, and P. Schwindt, *Rev. Sci. Instrum.* **82**, 023118 (2011).
- ¹³J. Noriega, L. Garcia-Delgado, R. Gomez-Fuentes, and A. Garcia-Juarez, *Rev. Sci. Instrum.* **87**, 094704 (2016).
- ¹⁴D. J. Berkeland, J. Miller, J. Bergquist, W. Itano, and D. Wineland, *J. Appl. Phys.* **83**, 5025 (1998).
- ¹⁵J. Keller, H. L. Partner, T. Burgermeister, and T. E. Mehlstäubler, *J. Appl. Phys.* **118**, 104501 (2015).
- ¹⁶C. Sias and M. Köhl, in *Quantum Gas Experiments—Exploring Manybody States*, edited by P. Törmä and K. Sengstock (Imperial College Press, 2014), Chap. 12.
- ¹⁷K. Johnson, J. Wong-Campos, A. Restelli, K. Landsman, B. Neyenhuis, J. Mizrahi, and C. Monroe, *Rev. Sci. Instrum.* **87**, 053110 (2016).
- ¹⁸C. Schneider, M. Enderlein, T. Huber, and T. Schaetz, *Nat. Photonics* **4**, 772 (2010).
- ¹⁹See <http://www.lens.unifi.it/ew/dwl.php?dwl=bm90ZXNmUkZ0cmFwRHJpdmUucGRm&mtyp=application/pdf> for the full schematics of the RF drive which can be downloaded at the link.
- ²⁰E. Perego, M. Pomponio, A. Detti, L. Duca, C. Sias, and C. Calosso, *Rev. Sci. Instrum.* **89**, 113116 (2018).
- ²¹D. Gandolfi, M. Niedermayr, M. Kumph, M. Brownnutt, and R. Blatt, *Rev. Sci. Instrum.* **83**, 084705 (2012).
- ²²R. Wester, *J. Phys. B: At., Mol. Opt. Phys.* **42**, 154001 (2009).